UAV-Aided Post-Disaster Cellular Networks: A Novel Stochastic Geometry Approach

Maurilio Matracia, *Student Member, IEEE*, Mustafa A. Kishk, *Member, IEEE*, and Mohamed-Slim Alouini, *Fellow, IEEE*

***Abstract*—Motivated by the need for ubiquitous and reliable communications in post-disaster emergency management systems (EMSs), we hereby present a novel and efficient stochastic geometry (SG) framework. This mathematical model is specifically designed to evaluate the quality of service (QoS) experienced by a typical ground user equipment (UE) residing either inside or outside a generic area affected by a calamity. In particular, we model the functioning terrestrial base stations (TBSs) as an inhomogeneous Poisson point process (IPPP), and assume that a given number of uniformly distributed unmanned aerial vehicles (UAVs) equipped with cellular transceivers is deployed in order to compensate for the damage suffered by some of the existing TBSs. The downlink (DL) coverage probability is then derived based on the maximum average received power association policy and the assumption of Nakagami-*m* fading conditions for all wireless links. The proposed numerical results show insightful trends in terms of coverage probability, depending on: distance of the UE from the disaster epicenter, disaster radius, quality of resilience (QoR) of the terrestrial network, and fleet of deployed ad-hoc aerial base stations (ABSs). The aim of this paper is therefore to prove the effectiveness of vertical heterogeneous networks (VHetNets) in emergency scenarios, which can both stimulate the involved authorities for their implementation and inspire researchers to further investigate related problems.**

***Index Terms*—Coverage analysis, stochastic geometry, binomial point process, UAVs, quality of resilience, post-disaster communications.**

I. Introduction

DISASTERS represent of the main threats to modern communities, because they can potentially compromise every form of life within the region involved, apart from the risk of damaging its economy and cultural heritage. Contextually, the United Nations (UN) established the International Search and Rescue Advisory Group (INSARAG) in 1991 in order to essentially [1]:

1) Improve the effectiveness of emergency preparedness and response operations;
2) Design activities that improve search-and-rescue (SAR) missions in disaster-prone countries;
3) Ameliorate cooperation among international urban-SAR (USAR) teams and develop procedures and systems for national teams operating internationally;
4) Develop USAR procedures, guidelines and best practices for the emergency relief phase.

Emergency situations often require reliable cellular coverage over large areas to ensure the safety of victims and first responders (FRs), especially during SAR missions. However, telecom infrastructure dysfunction (e.g., failure or lack of power supply) is one of the main concerns related to current network architectures. Indeed, the quality of telecommunications usually decreases after the occurrence of a disaster. Perturbations to the networking equipment can often lead to continuous reconfiguration of the routing tables, a larger ratio of packet losses, disturbances to radio frequency (RF) signals, and many other issues [2], [3]. Consequently, ABSs consisting of UAVs equipped with cellular transceivers are gaining more and more attention as an alternative solution for supporting TBSs in post-disaster scenarios [3], [4]. The latter, in fact, are generally susceptible to earthquakes, tornadoes, explosions, and many other serious perturbations.

Apart from their mobility, using ABSs as ad-hoc nodes in emergency situations is also more appropriate than using cell towers because of their lower cost, faster deployment, and higher altitude [5]. By reaching a higher altitude, indeed, it is possible for a BS to achieve a larger footprint as well as a higher probability of establishing line-of-sight (LoS) transmissions, which can generally lead to better communication channels compared to the case of non-LoS (NLoS) transmissions [6]. Furthermore, promising advancements in avionics and especially drone technology have enabled the use of such vehicles for several purposes (including disaster monitoring [7], damage assessment [8], and first aid and supply delivery [9], for instance), although their flight time is considerably reduced whenever operating in multi-task mode. However, there are many types of vehicles that can be used as ABSs: these are usually categorized as low-altitude platforms (LAPs) and high-altitude platforms (HAPs) [4]. Drones (either tethered [10], [11] or untethered) and tethered balloons are common examples of LAPs, and usually their altitude does not exceed 10 km. On the other hand, airships, gliders, and untethered balloons fall in the category of HAPs, since they are usually designed to operate in the stratosphere.

In this paper, we consider both LAPs and HAPs as a potential solution for supporting post-disaster communications while capturing the resiliency of the terrestrial cellular infrastructure.

Manuscript received 5 August 2022; revised 16 February 2023; accepted 19 February 2023. Date of publication 22 February 2023; date of current version 18 July 2023. This paper was supported by KAUST. The review of this article was coordinated by Dr. Tao Dusit Niyato. *(Corresponding author: Maurilio Matracia.)*

Maurilio Matracia and Mohamed-Slim Alouini are with the Computer, Electrical and Mathematical Sciences and Engineering (CEMSE) Division, King Abdullah University of Science and Technology (KAUST), Thuwal 23955, Saudi Arabia (e-mail: maurilio.matracia@kaust.edu.sa; slim.alouini@kaust.edu.sa).

Mustafa A. Kishk is with the Department of Electronic Engineering, Maynooth University, W23 F2H6 Maynooth, Ireland (e-mail: mkishk@vt.edu).

Digital Object Identifier 10.1109/TVT.2023.3247920

Given the inherent randomness of the network nodes' deployment and resilience, for our analysis we decided to implement an SG approach due to its tractability and accuracy.

More details on the contributions of this work are provided in Section I-B.

A. Related Works

This subsection provides a concise summary of the relevant literature works on UAV-assisted disaster communications and SG-based analysis of UAV networks.

1) UAV-Aided Disaster Communications: As explained in [12], the importance of UAVs in emergency scenarios is not limited to post-disaster situations but also concerns the phases of pre-disaster preparedness and disaster assessment. Indeed, many works in the literature discussing disaster communications have considered using UAVs for applications related to situational awareness [13], damage assessment [14], and network rehabilitation [4], [15], [16]. Authors in [13], in fact, approached the problem of situational awareness by deploying drones in order to capture a digital terrain model and place sensors in a disaster-struck area, creating a dynamic sensor network. On the other hand, [14] proposed combining UAV-based imagery with ground observations and collaborative sharing with domain experts for either post-disaster assessment, environmental management, or monitoring of infrastructure development. However, the most interesting application for UAVs in disaster scenarios is probably to support or even substitute the terrestrial cellular infrastructure, as respectively suggested in [15] and [16].

Finally, it is worth mentioning the current research interest in achieving UAVs' minimum energy consumption and optimal placement. For example, the work presented in [17] introduced the first multi-layered heterogeneous network architecture that integrates ad hoc UAVs into public safety communications; in particular, said architecture is expected to enable reliable communications in basements by means of both wired and wireless links. On the other side, in [18] a novel multi-objective integer linear optimization problem (ILP) was solved in order to optimally deploy the UAVs assisting disaster-affected users; the authors compared the branch-and-bound (B & B) algorithm with their proposed low-complexity heuristic one.

For a more detailed overview of this topic, the reader can refer to Ref. [3].

2) SG for UAV-Assisted Networks: During the last decade, SG has emerged in the literature as one of the most effective mathematical tools for modeling and analyzing large scale VHetNets. More specifically, the performances of UAV-assisted terrestrial cellular networks have been evaluated via SG approaches in works such as [19], [20], [21], [22], [23].

Arshad et al. [19] proposed an architecture consisting of macro and small TBSs supported by ABSs for evaluating the QoS experienced by either stationary or mobile users (by taking into account the effect of handover rates). Moreover, a setup with TBSs and ABSs modeled by means of distinct homogeneous Poisson point processes (HPPPs) was introduced in [20] in order to derive both the coverage probability and average data rate experienced by a typical ground UE. Following the same lines, in [21] we used two different Poisson point processes (PPPs) to model the aerial and terrestrial nodes, and introduced specific features such as the aerial exclusion zone and the inhomogeneous distribution of the TBSs' density to accurately model comprehensive environments that include both urban and exurban areas.

Furthermore, authors in [22] relied on SG to evaluate the effectiveness of ABSs, modeled as a binomial point process (BPP), while taking into account also the backhaul probability. Finally, we consider [23] as the most related work since it is the only one modeling also the resilience of the terrestrial nodes, which is done by introducing a thinning probability for the PPP-distributed TBSs. However, for the sake of simplicity, the latter work assumed the damages to spread over the entire ground plane, which may not be accurate for typical post-disaster scenarios.

B. Contributions

The contributions of our paper involve multiple aspects, as explained in this subsection.

1) System Model: We consider a large-scale post-disaster wireless network consisting of both terrestrial and aerial nodes. We devise accurate inhomogeneous PPPs (IPPPs) to model the planar distribution of the functioning TBSs (that is, we assume that the original distribution is thinned according to a certain probability depending on the distance from the disaster epicenter), both inside and outside a circular disaster-struck zone, whereas the aerial network is modeled as a BPP confined to the vertical projection of the disaster area.

Thus, the length of the disaster radius and the behavior of the QoR of the terrestrial network represent crucial parameters since they allow to capture the severity of any catastrophic event [4]. This, in turn, has an influence on the optimal fleet of ABSs (identified by number and the type of ad hoc nodes required to provide the highest QoS).

In conclusion, we consider our system model as a contribution to the existing literature because it takes into account both the vertical heterogeneity (due to the presence of aerial and terrestrial BSs) and the horizontal heterogeneity (due to the distribution of the surviving TBSs and the consequent placement of the ABSs) of integrated post-disaster wireless networks in an original way.

2) Performance Analysis: To the best of our knowledge, this paper provides the first SG-based framework specifically designed to analyze the DL performances of 5 G and beyond cellular VHetNets affected by a localized disaster while taking into account the QoR of the terrestrial infrastructure. Also, our framework is more general compared to the baseline ones [24], [25], since it allows to evaluate the performance of the network even when the user is outside the ground projection of the considered BPP's domain.

More specifically, the devised framework introduces a new method that makes use of indicator functions in order to avoid bulky piecewise expressions for describing the novel cumulative distribution functions (CDFs), probability density functions (PDFs), and Laplace transforms of the interference derived for

TABLE I
MAIN SUBSCRIPTS

Notation	Description	Definition
A	ABSs	—
T	Functioning TBSs	—
O	Generic type of BSs	$A \oplus T$
B	Type of tagged BS	$B \in \{A,T\} \ \wedge \ Q_B^* > Q_O^*, \ \forall O \neq B$
C	Type of interfering BSs	$C \in \{A,T\} \ \wedge \ Q_{C,W_i} < Q_B^*, \ \forall W_i \neq W^*$

each layer. In other words, compared to the methods available in the literature [20], [21], [25], this one better conveys the meaning of the derived expressions and eases their numerical implementation.

We applied our method to compute the *s*patial coverage probability (that is, we focus on covering an area independently from the actual distribution of the users), and validated the results via Monte Carlo simulations. In addition to better conveying the meaning of the derived expressions and easing their numerical implementation, another advantage of our method is its generality: indeed, the proposed expressions hold irrespective of the UE's location, whereas the conventional approaches would require different expressions depending on whether the typical user resides inside or outside the disaster-struck area.

3) System-Level Insights: Several fruitful insights can be extracted by investigating the behavior of the coverage probability in response to the considered parameters. For example, the obtained results show that the type and cardinality of a fleet of ABSs have a strong influence on the coverage probability, and should be optimized based on topological aspects such as the state of the terrestrial infrastructure, the disaster radius, and the typical UE's location. Indeed, even when neglecting the strict technological and economic constraints (e.g., UAVs' autonomy and backhaul, as well as their availability and associated cost of deployment), exploiting dense VHetNets imposes a trade-off between offering a strong desired signal and causing considerable interference to the UE.

II. System Model

A. Network Model

We consider a post-disaster scenario where the DL cellular network infrastructure is affected by a disaster, and thus a fleet of ad-hoc ABSs is deployed in order to make up for the failure of some TBSs within the suffered region. For the sake of both conciseness and readability we introduce a specific notation for the types of BSs, in accordance with Table I (where Q denotes the average received power and W the location of the BS).

Without any loss of generality, we set the origin $\boldsymbol{O}$ at the epicenter of the disaster. The disaster area is assumed with altitude 0, circular with radius r_d, and can thus be expressed as $\mathcal{A}_d = \mathbf{b}(\boldsymbol{O}, 0, r_d) \subset \mathbb{R}_0^2$, where $\mathbb{R}_0^2$ is the Euclidean ground plane.

As in the absence of any calamity the TBSs' planar distribution can generally be modeled by means of an HPPP [20], [26] of intensity $\lambda_0 > 0$, we hereby assume that the original infrastructure experience random failures within the disaster-struck area. Therefore, the IPPP $\Phi_T \equiv \{Y_i\} \subseteq \mathbb{R}_0^2$ describes the surviving TBSs' distribution; the intensity of this process is $\lambda_T(r) = \lambda_0 \left(\chi(r) \, \mathbb{1}(r \leq r_d) + \mathbb{1}(r > r_d)\right)$, where $r > 0$ represents the horizontal distance from the origin and $\chi(r) \in [0,1]$ identifies the QoR of the terrestrial network.

Finally, since the number of deployed UAVs decided by the authority is supposedly deterministic, the ABSs' planar distribution is described by means of a uniform binomial point process (BPP) $\Phi_A \equiv \{X_i\} \subseteq \mathcal{A}_h$, where $\mathcal{A}_h = \mathbf{b}(\boldsymbol{O}, h, r_d)$ indicates the vertical projection at altitude h of $\mathcal{A}_d$ (see Fig. 1). Although ABSs may definitely be subject to failures (especially in case of harsh weather conditions), we henceforth consider them totally resilient, because their deployment would occur after the actual disaster.

B. Channel Model

This subsection aims to characterize both the terrestrial and aerial wireless channels. Keeping in mind Table I, we assume that the signals transmitted by any BSs belonging to a given tier O have a fixed, constant transmit power ρ_O and experience standard power-law path loss propagation with path loss exponent $\alpha_O \geq 2$.

Let η denote the mean additional transmission losses, then we can define $\xi_O = \eta_O \, \rho_O$. We assume both the terrestrial and aerial links experience small-scale fading in the form of a Nakagami-*m* distribution with generic shape parameter m_O. Note that small-scale fadings are usually Rayleigh or Rician distributed. However, the Nakagami-*m* distribution with shape parameter $m = \frac{(K+1)^2}{2K+1}$ (and scale parameter equal to its reciprocal) allows a fair approximation of the Rician distribution with factor K [20]. For every $W_i \in \Phi_O$, the channel fading power gains G_{O,W_i}'s follow a Gamma distribution with PDF given by

$$f_{G_O,W_i}(g) = \frac{m_O^{m_O} \, g^{m_O - 1}}{\Gamma(m_O)} \, e^{-m_O \, g}, \tag{1}$$

where $\Gamma(m) = \int_0^\infty x^{m-1} \, e^{-x} \, \mathrm{d}x$ identifies the Gamma function.

For a given tier O, let Q_O denote the random variable referring to the average power received by the typical UE. We define Q_O^* and Q_{O,W_i} as the received powers coming from the closest and any generic O-BSs located at point W_i, respectively. Thus, the random power received by the typical user from a BS located at W_i can be expressed as

$$Q_{O,W_i} = \xi_O \, G_{O,W_i} \, (1 + D_{W_i})^{-\alpha_O} \approx \xi_O \, G_{O,W_i} \, D_{W_i}^{-\alpha_O}, \tag{2}$$

where we introduced the *m*odified path loss to formally avoid the absurdity $Q_{O,W_i} > \xi_O$, occurring for $D_{W_i} < 1$ m; nonetheless, we will (fairly) use the above approximation as we are considering large scale networks. Finally note that if $O = T$ then $D_{W_i} = \Omega_{W_i}$.

C. Association Policy

In this paper, the strongest average received power association rule is adopted, meaning that the user connects to the BS providing the highest average received power. This, however, does not exclude the possibility of having interferers providing higher received powers during a given instant. Moreover, due to the fact that each type of BS is characterized by a specific path-loss exponent, mean additional transmit losses, and transmit power,

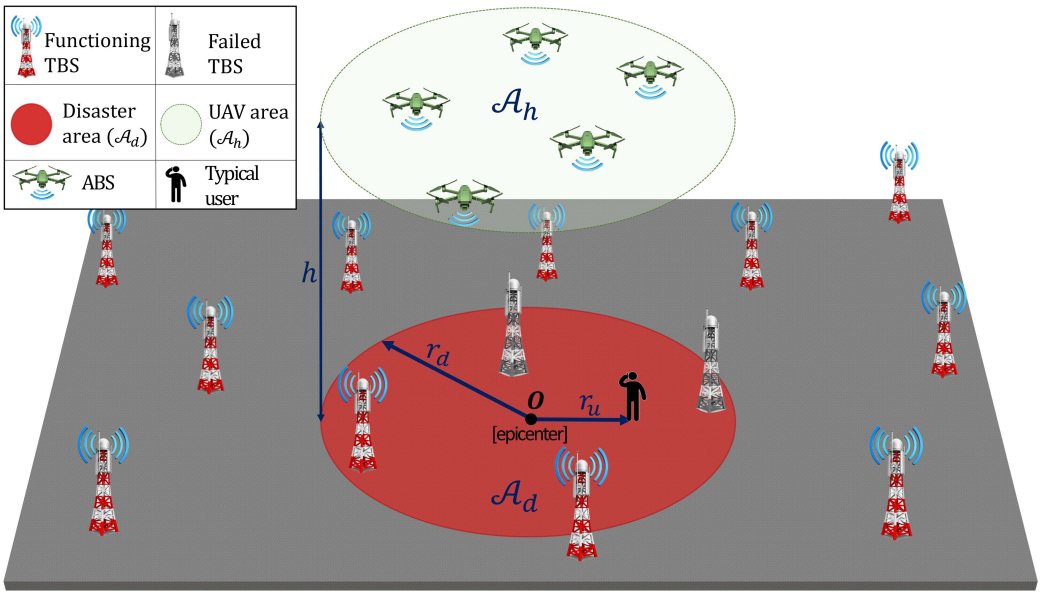

Fig. 1. Schematic representation of the system setup considered: the typical user is located at distance r_u from the epicenter of the disaster (i.e., the origin) and associates to the BS that provides the maximum average received power. All the failed TBSs belong to a circular disaster-struck region $\mathcal{A}_d$, whereas a fixed number of UAVs reside within its projection $\mathcal{A}_h$.

the serving BS is guaranteed to be the closest BS but only among the BSs of the same type.

Finally, we assume the expected values of the fading gains over all the sets of BSs (i.e., $\mathbb{E}[G_{O,W_i}], \forall W_i \in \Phi_O$) to equal 1. Hence, the location of the tagged BS will be simply provided by the maximum product $\xi_O \, D_{O,W_i}^{\alpha_O}$, that is

$$W^* = \underset{W_i \in \Phi_O}{\arg\max} \left(\xi_O \, D_{O,W_i}^{-\alpha_O} \right), \forall O \in \{A, T\}. \tag{3}$$

D. Interference and Signal-to-Interference-Plus-Noise Ratio (SINR)

The instantaneous SINR can be expressed as

$$\mathrm{SINR} = \frac{Q_B^*}{\sigma_n^2 + I}, \tag{4}$$

where σ_n^2 is the additive white Gaussian noise (AWGN) power and I is the aggregate interference power. Letting C denote the layer hosting each interfering BS and assuming that all BSs share the same frequency or time resource blocks, then the random variable (RV) I can be introduced as

$$I = \sum_{C=\{A,T\}} \sum_{\substack{W_i \in \Phi_C \\ W_i \neq W^*}} Q_{C,W_i}. \tag{5}$$

E. Coverage Probability

The coverage probability is defined as the complementary cumulative distribution function (CCDF) of the SINR evaluated at a designated threshold τ ensuring reliable decoding, that is

$$P_c = \mathbb{P}(\mathrm{SINR} > \tau). \tag{6}$$

III. Performance Analysis

In this section, the distributions of the distance to the closest O-BS, the association probabilities, and the conditional Laplace transforms of the interference will be derived for both the aerial and terrestrial layers of BSs in order to obtain the approximate and exact expressions of the coverage probability.

A. Distance to the Nearest O-BS

Intuitively, the coverage probability is a function of the distance between the UE and the tagged BS. In order to derive the exact and approximate expressions of the coverage probability, the theorems in this subsection characterize the distribution of the horizontal distance between the UE and each closest O-BS by computing its CDF. Consequently, the respective PDF will be derived in a corollary.

Theorem 1: Let r_u be the distance between the typical user and the center of a disaster with radius r_d, then the CDF of the random horizontal distance[1] Z_T between the UE and the closest TBS in an IPPP with density $\lambda_T(r)$ is given by

$$F_{Z_T}(z) = 1 - \exp\left(- \int_0^{2\pi} \int_0^{z} \lambda_T \left(r_\Omega(\omega, \beta) \right) \omega \, \mathrm{d}\omega \, \mathrm{d}\beta \right), \tag{7}$$

where $r_\Omega(\omega, \beta) = \sqrt{r_u^2 + \omega^2 - 2\, r_u\, \omega \, \cos\beta}$ describes the ground distance from the origin.

Proof: See Appendix A. ■

Corollary 1: Henceforth, let the overline characterize the complementary functions (i.e., $\bar{F}_{Z_O}(z) = 1 - F_{Z_O}(z)$). The

[1] Whenever not specified, we always refer to the distance from the typical UE, around which the polar coordinate system (ω, β) is centered.

PDF of the distance Z_T between the UE and the closest surviving TBS is

$$f_{Z_T}(z) = z\,\bar{F}_{Z_T}(z)\int_0^{2\pi}\lambda_T\left(r_\Omega(z,\beta)\right)\,\mathrm{d}\beta\,. \tag{8}$$

Proof: See Appendix B. ∎

Due to the inherent complexity of the BPP, the distance distribution to the closest ABS cannot be computed directly. Therefore, as an intermediate step, we now leverage a well-known property of BPPs in order to obtain the distribution of the horizontal distance Ω_A between the UE and any ABS.

Proposition 1: For a given set of N points uniformly distributed over an area $\mathcal{A}$, the points residing in any subarea $\Sigma \subseteq \mathcal{A}$ are uniformly distributed with cardinality $n \sim \mathrm{Bin}(N, \frac{\Sigma}{\mathcal{A}})$ [27, Theorem 2.9].

Lemma 1: In accordance to [25, Lemma 1], the horizontal distances Ω_A's to the set of independently and uniformly distributed UAVs are independent and identically distributed (iid), with the CDF and PDF of each element respectively given by

$$F_{\Omega_A}(\omega) = \frac{\Sigma(\omega)}{\mathcal{A}_d}\,, \tag{9}$$

and

$$f_{\Omega_A}(\omega) = \frac{1}{\mathcal{A}_d}\,\frac{\mathrm{d}\Sigma(\omega)}{\mathrm{d}\omega}\,, \tag{10}$$

in which $\Sigma(\omega) = \int_0^{2\pi}\int_0^{\omega}\mathbb{1}(r_\Omega(\omega,'\beta) < r_d)\,\omega'\,\mathrm{d}\omega'\,\mathrm{d}\beta$ describes the intersection area between $\mathcal{A}_d$ and the disc of radius ω centered around the UE, and $\frac{\mathrm{d}\Sigma(\omega)}{\mathrm{d}\omega} = \omega\int_0^{2\pi}\mathbb{1}(r_\Omega(\omega,\beta) < r_d)\,\mathrm{d}\beta$.

Proof: The expression of $\frac{\mathrm{d}\Sigma(\omega)}{\mathrm{d}\omega}$ can be easily derived by applying the Leibniz rule to $\Sigma(\omega)$. ∎

These latter results allow us to extract the distribution of the respective minimum horizontal distance Z_A, as shown in what follows.

Theorem 2: Let N_A denote the number of deployed UAV-mounted BSs, then the CDF of the closest horizontal distance to a UAV is [24]

$$F_{Z_A}(z) = 1 - \bar{F}^{N_A}_{\Omega_A}(z)\,. \tag{11}$$

Proof: Since $Z_A = \min_i\{\Omega_{A,i}\}$, then we can derive its CDF as

$$\begin{aligned} F_{Z_A}(z) &= \mathbb{P}(Z \le z) = 1 - \mathbb{P}\left(\min_i\{\Omega_{A,i}\} > z\right) \\ &= 1 - \bar{F}^{N_A}_{\Omega_A}(z). \end{aligned}$$

∎

Corollary 2: The PDF of the closest ground distance to a UAV is

$$f_{Z_A}(z) = N_A\,\bar{F}^{N_A-1}_{\Omega_A}(z)\,f_{\Omega_A}(z)\,. \tag{12}$$

Proof: The result trivially follows from taking the derivative of $F_{Z_A}(z)$ with respect to z. ∎

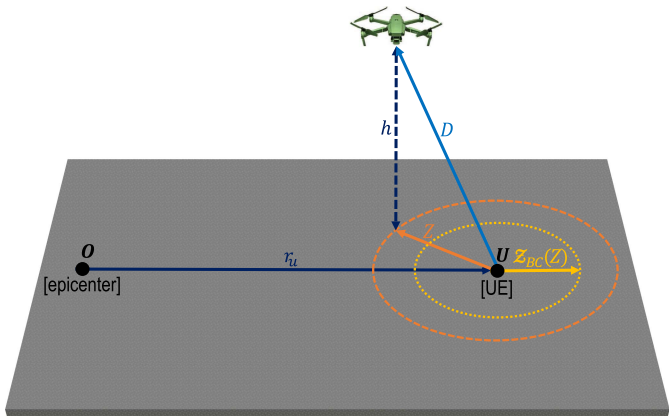

Fig. 2. Generic representation of the minimum interferer horizontal distance $\mathcal{Z}_{BC}(Z)$ in relation to the Euclidean and horizontal distances to the closest B-BS. Note also that, for the sake of an easier representation, the minimum interferer distance $\mathcal{D}_{BC}(Z)$ has been omitted.

B. Association Probabilities

The B-association probability quantifies the likelihood that the UE associates to an B-BS. Based on our assumptions, this can be computed as the probability that the maximum average received power comes from the closest B-BS, as conveyed in the following theorem.

Theorem 3: Recalling the subscripts defined in Table I, we denote as $\mathcal{D}_{BC}(z)$ the minimum Euclidean distance of any C-interferer if the user associates to a B-BS situated at ground distance z. Consequently, $\mathcal{Z}_{BC}(z) = \begin{cases}\sqrt{\mathcal{D}^2_{BC}(z) - h^2}, & \text{if } C = A\\ \mathcal{D}_{BC}(z), & \text{if } C = T\end{cases}$ expresses the horizontal projection of $\mathcal{D}_{BC}(z)$ (see Fig. 2). Let $r^{\pm} = r_d \pm r_u$, $\mathcal{R}_T = [0,\infty[$, and $\mathcal{R}_A = [\max(0, -r^-), r^+]$,[2] then each B-association probability can be expressed as

$$\mathcal{A}_B = \int_{\mathcal{R}_B} f_{Z_B}(z)\,a_B(z)\,\mathrm{d}z\,, \tag{13}$$

where $a_B(z) = \prod_{C\neq B}\bar{F}_{Z_C}(\mathcal{Z}_{BC}(z))$ represents the association probability conditioned on the association to a B-BS, which we refer to as the conditional B-association probability.

Proof: See Appendix C. ∎

C. Conditional Laplace Transforms of the Interference

Assuming that all BSs operate within the same frequency band, it follows that co-channel interference is generated by each BS except the tagged one. Therefore, it is possible to characterize the interference statistics by computing the Laplace transform of the RV I, which denotes the aggregate interference. To this extent, the theorems in this subsection preliminary provide the expressions of the conditional Laplace transforms of the interference generated by each tier of base stations (BSs).

[2] It is evident that the first argument of $\max(x, y)$ is chosen if and only if the user is located inside $\mathcal{A}_d$.

Again, the first result we propose refers to the working TBSs, now considered as interferers in the following theorem.

Theorem 4: By recalling the expression of $r_\Omega(\omega,\beta)$ from Theorem 1, the conditional Laplace transform of the interference due to TBSs can be expressed as

$$\mathcal{L}_{I_{BT}}(s|z) = \exp\left(-\int_0^{2\pi}\int_{\mathcal{Z}_{BT}(z)}^{\infty} \lambda_T\left(r_\Omega(\breve{\omega},\beta)\right) \times \mathcal{I}_T(s|\breve{\omega})\,\breve{\omega}\,\mathrm{d}\breve{\omega}\,\mathrm{d}\beta\right), \tag{14}$$

where $\mathcal{I}_T(s|\omega) = 1 - \left(\frac{m_T}{m_T+\xi_T\, s\,\omega^{-\alpha_T}}\right)^{m_T}$.

Proof: See Appendix D. ∎

Again, due to the greater complexity of the BPP compared to the PPP, an intermediate step is required to obtain the conditional Laplace transform of the interference coming from the aerial nodes. To this extent, the following lemma defines the expression of the PDF of the horizontal distance $\breve{\Omega}_A$ between the UE and any interfering ABS.

Lemma 2: Let $r^+ = r_d + r_u$, then the aerial interferers' horizontal distances $\breve{\Omega}_{A,i}$'s constitute an unordered set of iid RVs with PDF expressed as

$$f_{\breve{\Omega}_A}(\breve{\omega}|z) = \frac{f_{\Omega_A}(\breve{\omega})}{\bar{F}_{\Omega_A}(z)},\ z \le \breve{\omega} \le r^+. \tag{15}$$

Proof: Let us preliminarily define $n_1 = 1 + \mathbb{1}(B=A)$ and $\breve{N}_A = N_A - \mathbb{1}(B=A)$. Then, the conditional joint PDF of the aerial interferers' horizontal distances is

$$f_{\breve{\Omega}_{BA,i}}(\breve{\omega}_{n_1},\ldots,\breve{\omega}_{N_A}|z) \overset{(a)}{=} \frac{N_A!\, f_{\Omega_A}(z)\prod_{i=n_1}^{N_A} f_{\Omega_A}(\breve{\omega}_i)}{f_{Z_A}(z)\,\bar{F}_{\Omega_A}^{\mathbb{1}(B\neq A)}(z)} \overset{(b)}{=} \breve{N}_A!\prod_{i=n_1}^{N_A}\frac{f_{\Omega_A}(\breve{\omega}_i)}{\bar{F}_{\Omega_A}(z)}, \tag{16}$$

where (a) follows from the joint PDF for the order statistics of a sample of size N_A drawn from the distribution of Ω_A [25, Appendix C], and (b) follows by expressing the term $f_{Z_A}(z)$ as in (12). By recalling [24, Lemma 3], we notice that the factorial term $(N_A-1)!$ indicates all possible permutations of the elements in the ordered set of the aerial interferers' horizontal distances. As a result, by the joint PDF of the ground distances in the ordered set, the corresponding ground distances in the unordered set are iid with PDF given by (15). ∎

As already anticipated, we can now express the conditional Laplace transform of the aerial interference by means of the following theorem.

Theorem 5: The conditional Laplace transform of the interference due to the ABSs in the case of B-association can be expressed as

$$\mathcal{L}_{I_{BA}}(s|z) = \Upsilon_{BA}^{\breve{N}_A}(s,z), \tag{17}$$

where $\Upsilon_{BA}(s,z) = \int_{\mathcal{Z}_{BA}(z)}^{r^+} \mathcal{I}_A(s|\breve{\omega})\, f_{\breve{\Omega}_A}(\breve{\omega}|\mathcal{Z}_{BA}(z))\,\mathrm{d}\breve{\omega}$ with $\mathcal{I}_A(s|\breve{\omega}) = \left(\frac{m_A}{m_A+\xi_A\, s\,\mathcal{D}_{AA}^{-\alpha_A}(\breve{\omega})}\right)^{m_A}$.

Proof: See Appendix E. ∎

To conclude, the following corollary defines the conditional Laplace transform of the aggregate interference.

Corollary 3: The conditional Laplace transform of the aggregate interference can be expressed as

$$\mathcal{L}_{I,B}(s|z) = \prod_{C=\{A,T\}} \mathcal{L}_{I_{BC}}(s|z). \tag{18}$$

Proof: The proof trivially follows by recalling that the aggregate interference is the sum of the interferences coming from each layer. ∎

D. Coverage Probability

Based on the expressions derived for the PDFs of the distance to the closest BS, the conditional association probabilities, the SINR, and the Laplace transform of the interference, we hereby provide the exact and approximate expressions of the coverage probability under Nakagami-m fading conditions.

Theorem 6: Let $p_{c,B}(z)$ denote the exact coverage probability conditioned on the association to a B-BS located at horizontal distance z within its own planar domain $\mathcal{R}_B$ defined as in Theorem 3. Then, the exact coverage probability for a typical user in the wireless system described in Section II is given by

$$P_c = \sum_{B=\{A,T\}} \int_{\mathcal{R}_B} a_B(z)\, p_{c,B}(z)\, f_{Z_B}(z)\,\mathrm{d}z, \tag{19}$$

where

$$p_{c,B}(z) = \sum_{k=0}^{m_B-1} \frac{(-\mu_B(z))^k}{k!}\frac{\partial^k}{\partial s^k}\mathcal{L}_{J,B}(s|z)\Big|_{s=\mu_B(z)} \tag{20}$$

with $\mathcal{L}_{J,B}(s|z) = e^{-s\,\sigma_n^2}\,\mathcal{L}_{I,B}(s|z)$ and $\mu_B(z) = m_B\frac{\tau}{\xi_B}\mathcal{D}_{BB}^{\alpha_B}(z)$. The expressions of the functions $f_{Z_B}(z)$'s are provided in Corollaries 1 and 2; the general expression of the association probabilities $a_B(z)$'s is given by Theorem 3; the functions $\mathcal{L}_{I,B}(s|z)$'s respectively refer to Theorems 4 and 5.

Proof: See Appendix F. ∎

Since computing the exact expression of the conditional coverage probability may require computing high-order derivatives of the conditional Laplace transform of the interference, it is usually preferable to approximate it, as suggested by the following theorem.

Theorem 7: To ease the evaluation of the coverage probability, the conditional coverage probability can be approximated as [20, Section III-D]

$$\tilde{p}_{c,B}(z) = \sum_{k=1}^{m_B}\binom{m_B}{k}(-1)^{k+1}\,\mathcal{L}_{J,B}\left(k\,\varepsilon_{2,B}\,\mu_B(z),z\right), \tag{21}$$

where $\mathcal{L}_{J,B}(s|z)$ and $\mu_B(z)$ are given by Theorem 6, and $\varepsilon_{2,B} = (m_B!)^{-\frac{1}{m_B}}$.

Proof: See Appendix G. ∎

TABLE II
MINIMUM INTERFERER DISTANCES $\mathcal{D}_{BC}(z)$

B \ C	T	A
T	z	$\begin{cases} \frac{\xi_A}{\xi_T}^{\frac{1}{\alpha_A}} z^{\frac{\alpha_T}{\alpha_A}}, & \text{if } z > \mathcal{D}_{AT}(0) \\ h, & \text{otherwise} \end{cases}$
A	$\frac{\xi_T}{\xi_A}^{\frac{1}{\alpha_T}} (\sqrt{z^2+h^2})^{\frac{\alpha_A}{\alpha_T}}$	$\sqrt{z^2+h^2}$

IV. RESULTS AND DISCUSSION

In this section, the analytical results based on the expressions derived in Section III are verified by means of Monte Carlo simulations. By inspecting these results, we will try to understand how each system parameter affects the network's performance as defined in Theorem 7 (or Theorem 6 when no ABSs are deployed). However, let us recall that we are: (i) assuming ideal backhaul links, (ii) evaluating the QoS only in terms of coverage probability, and (iii) for the sake of conciseness and mathematical tractability, not specifying the difference between LoS and NLoS transmissions for both the terrestrial and aerial tiers (this, however, is a precautionary assumption since the presence of NLoS nodes would strongly reduce the average aerial interference power without significantly increase the average desired signal power, leading to more optimistic behaviors of the coverage probability as the number of UAVs N_A is increased). Note also that aerial BSs present limitations in terms of capacity (e.g., due to the small number of antennas supported) and autonomy, which considerations are beyond the scope of this study. Nonetheless, the observed trends can effectively support cellular operators in network planning. For example, they would be able to quantify the advantage of strengthening the terrestrial infrastructure, as well as predicting the number of ad hoc ABSs needed in the occurrence of a specific calamity.

For this study, unless stated otherwise, we have assumed the values of the parameters according to Table III and used markers and lines to represent analysis and simulation results, respectively. Note also that, although the standard values of the disaster radius r_u and the QoR χ do not reflect typical disaster scenarios (since the majority of the users should be close to the edge of the disaster-struck area $\mathcal{A}_d$ and the network should not be fully destroyed), they may correspond to the most critical situation (since users at the disaster epicenter have more chances to be trapped and/or seriously injured, and a less resilient network has more chances of becoming overloaded).

A. Influence of the Disaster Radius

In Fig. 3, the impact of the disaster radius r_d is investigated under the assumption that either LAPs, HAPs, or none of them are deployed. In particular, the plots describe different coverage probability behaviors depending on the cardinality N_A of each type of fleet of ABSs. Different positive values of N_A have been selected for LAPs and HAPs because of their difference in terms of coverage area. Finally note that, to better highlight the influence of r_d, here we assume $\chi = 0$ and $r_u = 0$. From Fig. 3 we can extract some precious insights:

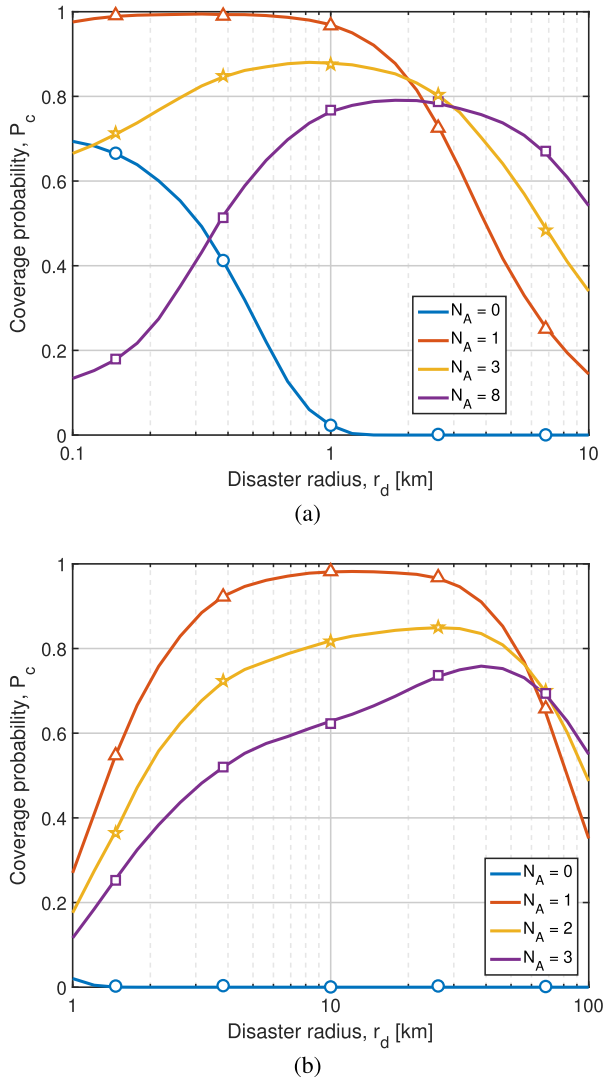

Fig. 3. Coverage probability as function of the disaster radius when the ABSs deployed are: (a) LAPs and (b) HAPs.

1) Outer TBSs: Based on the considered system parameters, outer TBSs can support the UE (assuming $r_u = 0$) only for very small values of r_d; in other words, P_c rapidly approaches zero as r_d exceeds a couple of hundred meters. This occurs because a larger disaster radius implies a longer average distance to the closest functioning TBS (which in this case is lower-bounded by r_u): in other words, the higher path loss overcompensates the weaker interference. Therefore, unless $\mathcal{A}_d$ is very small, non-resilient networks ($\chi = 0$) should not be considered self-sufficient.

2) LAPs: If r_d is less than two kilometers, deploying one single LAP is generally the optimal choice, as the red curve in Fig. 3(a) confirms. Our explanation to this fact relies in the well-known trade-off for VHetNets' densification: while increasing the number of nodes statistically reduces the distance to the tagged BS, it increases the power of the aggregate interference. However, for $r_d \geq 2$ km the optimal N_A rapidly increases: for $r_d = 10$ km even eight LAPs are not enough to ensure sufficient

TABLE III
MAIN SYSTEM PARAMETERS' STANDARD VALUES

Parameters	Values
Original TBSs' density	$\lambda_0 = 3\,\text{TBSs/km}^2 = 3\times10^{-6}\,\text{TBSs/m}^2$
ABSs' altitudes	$h = [0.2,\ 20]\,\text{km} = [200,\ 2\times10^4]\,\text{m}$, respectively for LAPs and HAPs
QoR	$\chi = 0$
UEs' distance from the origin	$r_u = 0$
Disaster radius	$r_d = [1,\ 10]\,\text{km}$, respectively for LAPs- and HAPs-based solution
Path loss exponents	$\alpha_A = [3,\ 2.5]$, respectively for LAPs and HAPs; $\alpha_T = 3.5$
Transmit powers	$\rho_A = [5,\ 50]$ W, respectively for LAPs and HAPs; $\rho_T = 10$ W
Nakagami-m shape parameters	$m_A = 2,\ m_T = 1$
SINR threshold	$\tau = -5\,\text{dB} = 0.3162$
Noise power	$\sigma_n^2 = 10^{-12}\,\text{W}$
Mean additional transmit losses	$\eta_A = -1.6\,\text{dB} = 0.6918,\ \eta_T = -2\,\text{dB} = 0.631$

reliability (for which we may expect $P_c \gtrapprox 0.6$) at the epicenter of the calamity.

3) HAPs: In case of relatively small disasters, deploying HAPs is highly discouraged, as Fig. 3(b) confirms. On the other side, as r_d exceeds a few kilometers, HAPs can be successfully deployed by leveraging their strong transmit power and favorable channel conditions. The optimal cardinality of the fleet is usually $N_A = 1$, but it rapidly increases as $r_d \to 100$ km: in fact, here the aerial interference experienced at the disaster epicenter becomes much less detrimental while a higher value of N_A generally implies a shorter distance between the UE and the closest HAP.

B. Influence of the UE's Location

In this subsection we investigate the influence, in terms of coverage probability, of the distance of the user with respect to the epicenter. This time, r_d is specifically fixed in order to simulate a typical disaster scenario for various LAPs- or HAPs-aided networks, which based on the results obtained in Fig. 3 (and also in our previous paper [4]) are assumed to be conveniently deployed in case of small or large disasters, respectively. Once again, we assume there are no surviving TBSs inside the disaster-struck zone.

1) Outer TBSs: As expected, the blue curves in Fig. 4 convey that the TBSs surrounding $\mathcal{A}_d$ can be quite effective in serving UEs located relatively close to the edge of the suffered region (roughly within a hundred meters). We can also see that the QoS experienced by the typical user slightly depends on r_d, and is mostly affected by the distance to the closest working TBS.

2) LAPs: Fig. 4(a) illustrates an overall improvement when deploying low-altitude aerial nodes above a relatively small disaster region of radius 1 km. We can notice that all the considered LAP fleets are able to cover more than twice the area of $\mathcal{A}_d$. In addition, for a typical user located at the origin the highest QoS is achieved for $N_A = 1$, as anticipated in Fig. 3(a).

For the considered setup, a high number of aerial nodes (see the violet curve) would not maximize the network performance for any distance from the epicenter, and therefore is not recommended. Finally, for outer UEs the aerial interference is quite negligible as long as $N_A \leq 3$, which would promote the

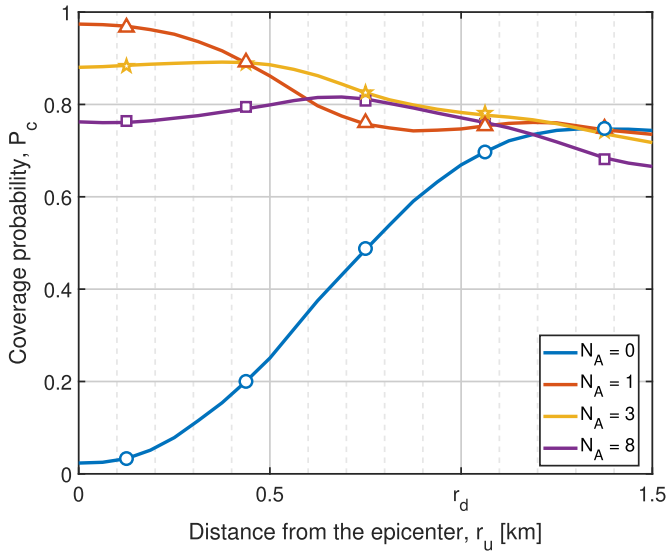

(a)

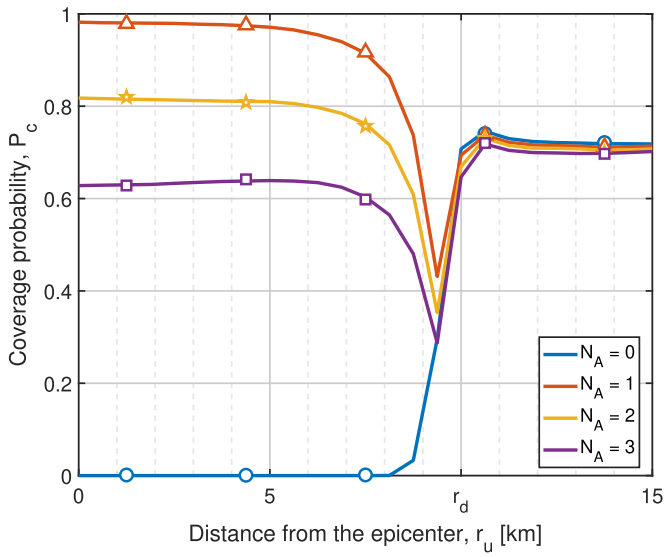

(b)

Fig. 4. Coverage probability as function of the UE's location when the ABSs deployed are: (a) LAPs and (b) HAPs. The disaster radius is assumed equal to one and ten kilometers, respectively.

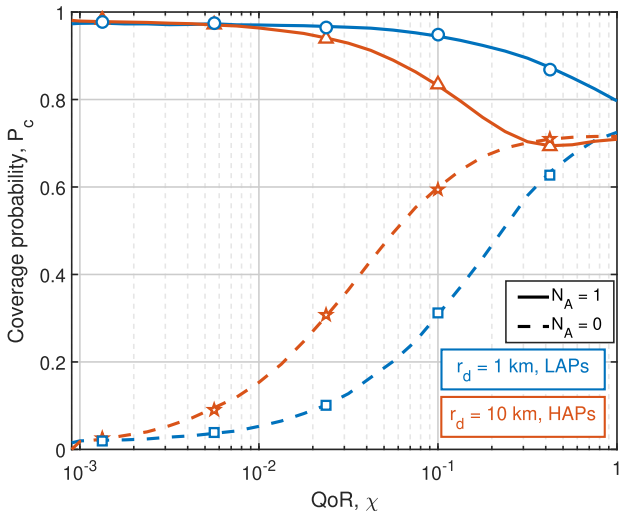

Fig. 5. Coverage probability as a function of the QoR (assumed uniform over the disaster-struck area) and the user is located at the origin.

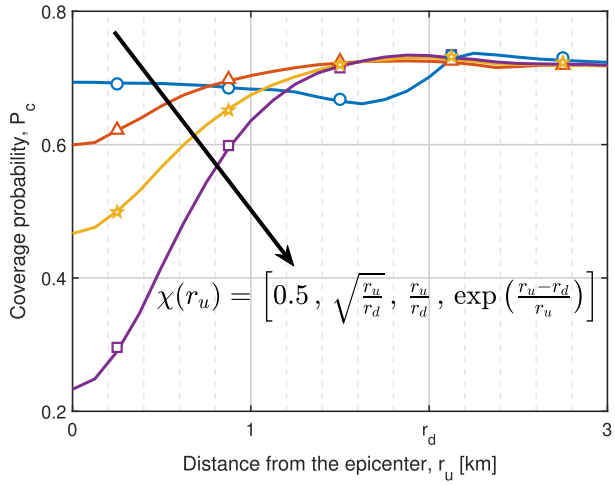

Fig. 6. Coverage probability as function of the UE's location for various QoR behaviors, considering $N_A = 0$ and $r_d = 2$ km.

deployment of multiple LAPs in case of a considerable traffic demand.

3) HAPs: For this scenario, we considered a disaster radius of 10 km. From Fig. 4(b), it is evident that deploying multiple HAPs is not convenient since it implies a strong aerial interference, although it might be needed in case of a considerably larger size of the disaster.

Furthermore, we can state that the users located around the epicenter are the ones which benefit the most from the deployed HAPs, up to the point that for $N_A \leq 2$ their experienced post-disaster QoS surpasses its pre-disaster counterpart. As the typical user moves away from the epicenter, the A-association generally decreases and the aerial interference becomes more and more problematic; then, a minimum coverage is experienced at around 600 m before the edge of $\mathcal{A}_d$, where the outer TBSs become close enough to frequently serve the user and the terrestrial interference dominates over its aerial counterpart.

C. Influence of the QoR

Let us now focus on the concept of resiliency by evaluating the coverage probability for various expressions of $\chi(r)$. We propose two studies to better understand the importance of having resilient TBSs: one assumes a uniform QoR and includes ABSs in the network architecture, whereas the other investigates various QoR's planar distributions while omitting ABSs.

1) Uniform QoR: The dashed curves of Fig. 5 tell us that, from a pure coverage perspective, if $N_A = 0$ then a small value of $\mathcal{A}_d$ can be much more problematic than a hundred times larger one. This can be explained by taking into account that a larger disaster area paradoxically benefits a typical user located at its epicenter because it increases the distance to the interfering outer TBSs. Instead, the solid lines show that even one single aerial node can lead to a high A-association probability (because of the advantaged channel conditions) and consequently boost the coverage probability, especially as $\chi \to 0$, which confirms the results previously shown in Figs. 3 and 4.

Generally speaking, P_c decreases or increases depending on whether the ABS (and especially the HAP) is present or not. As Fig. 5 illustrates, by assuming a fully-resilient terrestrial network (which is equivalent to the scenario without any perturbation) we would always have $0.7 < P_c < 0.8$, meaning that the aerial node would not remarkably improve the existing infrastructure. Actually, for $\chi \geq 0.4$ a small degradation of P_c due to the presence of a HAP can be observed by comparing the red curves.

2) QoR Distributions: We hereby consider a medium-size disaster with $r_d = 2$ km and investigate the behavior of P_c as a function of r_u. As a parameter, we consider various planar distributions (namely, constant, square-root-like, linear, and exponential with respect to r_u) of the QoR and compare them in the presence of only terrestrial nodes. The expression of $\chi(r_u)$ might strongly depend on the entity of the disaster: for example, we may expect an explosion leading to a sharp variation of the density of surviving TBSs as we move away from the origin, while a flood should have a more uniform influence on the surrounding environment.

All the curves displayed in Fig. 6 convey that, compared to the case with full TBS density (which can be fairly assumed if $r_u \gg r_d$), even halving the original TBS density (that is, reducing the QoR to just 0.5) would nowhere compromise the QoS, because r_d is relatively small. Consistently with Fig. 5, we can also notice that for $r_u \to 0$ the QoS directly depends on the local density $\lambda_T(r_u)$; in this scenario, the interference coming from the outer TBSs is usually negligible and the inner interferers are much farther than the tagged TBS. Instead, if the user is close to the edge of $\mathcal{A}_d$, the interference becomes relevant and hence a higher density of the surrounding TBSs leads to a slightly lower value of P_c.

V. Conclusion and Future Works

In this paper, we proposed a concise and tractable mathematical framework which borrows tools from SG and makes use of indicator functions in order to enable the estimation of the QoS

in UAV-assisted post-disaster wireless networks. In particular, given a typical VHetNet consisting of partially-resilient TBSs and ad-hoc ABS, we provided novel analytical expressions for the minimum distance distributions, association probabilities, and Laplace transforms of the interference in order to obtain the exact and approximate expressions of the coverage probability experienced by a typical UE, which can be arbitrarily located anywhere on the ground plane. Furthermore, by verifying the obtained numerical results, we proved that a properly chosen fleet of ad-hoc ABSs can strongly support the terrestrial infrastructure in various scenarios, and highlighted the trade-off between wider coverage and stronger interference due to heterogeneous network's densification.

This study could be extended in various research directions. For example, a more general setup where the ABSs operate in either LoS or NLoS condition with respect to the user should be considered in the future. Furthermore, it would be interesting to evaluate novel solutions for interference mitigation in post-disaster scenarios, perhaps by switching off some specific extra-region TBSs that are unlikely to serve any high-priority users involved in the disaster; this strategy would also help to reduce the overall power consumption, which is a critical issue since power systems are also susceptible to calamities. Finally, other important aspects such as network overload and backhaul issues could be taken into account in future extensions of this work.

Appendix A
Proof of Theorem 1

Recalling that the altitude of terrestrial antennas is assumed to be negligible compared to that of their aerial counterparts, the ground (and Euclidean) distance between the UE and the tagged TBS is identified by the RV Z_T. Thus, the expression of the respective CDF can be derived from the null probability of the PPP [26]. Let $N_T(z)$ be the number of TBSs residing within a distance z from the UE, then:

$$\begin{aligned} F_{Z_T}(z) &= \mathbb{P}(Z_T \leq z) = 1 - \mathbb{P}(Z_T > z) \\ &= 1 - \mathbb{P}(N_T(z) = 0) \\ &= 1 - \exp\left(- \int_0^{2\pi} \int_0^{z} \lambda_T \left(r_\Omega(\omega, \beta)\right) \, \omega \, \mathrm{d}\omega \, \mathrm{d}\beta \right), \end{aligned} \tag{22}$$

where $r_\Omega(\omega, \beta) = \sqrt{r_u^2 + \omega^2 - 2\, r_u\, \omega \, \cos\beta}$ and $\lambda_T(\omega, \beta)$ describe the horizontal distance from the origin and the behavior of the post-disaster TBSs' density, respectively.

Appendix B
Proof of Corollary 1

The derivative of $F_{Z_T}(z)$ is

$$\begin{aligned} f_{Z_T}(z) = \; & - \exp\left(- \int_0^{2\pi} \int_0^{z} \lambda_T \left(r_\Omega(\omega, \beta)\right) \, \omega \, \mathrm{d}\omega \, \mathrm{d}\beta \right) \\ & \times \left(- \frac{\mathrm{d}}{\mathrm{d}z} \int_0^{2\pi} \int_0^{z} \lambda_T \left(r_\Omega(\omega, \beta)\right) \, \omega \, \mathrm{d}\omega \, \mathrm{d}\beta \right), \end{aligned} \tag{23}$$

where, introducing $g_z(z, \beta) = \int_0^z \lambda_T(r_\Omega(\omega, \beta))\, \omega \, \mathrm{d}\omega$ and applying the Leibniz integral rule, we have

$$\begin{aligned} \frac{\mathrm{d}}{\mathrm{d}z} \int_0^{2\pi} g_z(z, \beta) \, \mathrm{d}\beta = \; & g_z(z, 2\pi) \, \frac{\mathrm{d}}{\mathrm{d}z}(2\pi) - g_z(z, 2\pi) \, \frac{\mathrm{d}}{\mathrm{d}z}(0) \\ & + \int_0^{2\pi} \frac{\partial}{\partial z} \, g_z(z, \beta) \, \mathrm{d}\beta \\ = \; & 0 - 0 + \int_0^{2\pi} \frac{\partial}{\partial z} g_z(z, \beta) \, \mathrm{d}\beta \\ = \; & z \int_0^{2\pi} \lambda_T \left(r_\Omega(z, \beta)\right) \, \mathrm{d}\beta, \end{aligned} \tag{24}$$

which completes the proof.

Appendix C
Proof of Theorem 3

The B-association probability represents the probability that the UE associates to a BS of type B (i.e., the average power received from the closest BS of type B exceeds the average powers received from the closest BSs of the other types).

Now, let $\mathcal{D}_{BC}(z)$ express the minimum Euclidean distance of any interfering BS of type C when the UE associates to a BS of type B located at ground distance z. Noting that the Euclidean distance to the tagged BS equals $\sqrt{z^2 + h^2}$ if $B = A$ and z otherwise, we define the projection on the ground of $\mathcal{D}_{BC}(z)$ as:

$$\mathcal{Z}_{BC}(z) = \begin{cases} \sqrt{\mathcal{D}_{BC}^2(z) - h^2}, & \text{if } C = A \\ \mathcal{D}_{BC}(z), & \text{if } C = T \end{cases},$$

which is conceptually represented in Fig. 2.

By recalling that $\xi_O = \rho_O \, \eta_O$ with $O \in \{A, T\}$, and introducing the random Euclidean distance $D_O = \mathcal{D}_{OO}(Z_O)$ as function of its own horizontal component Z_O, we can finally derive the B-association probabilities, as follows.

A. T-Association Probability

Recalling that Q_O^* denotes the average power received from the closest A- or T-BS, then the probability $\mathbb{P}(Q_T^* > Q_A^*)$ depends on Z_T, and hence

$$\mathcal{A}_T = \mathbb{P}\left(Z_A > \mathcal{Z}_{TA}(Z_T)\right) = \int_0^{\infty} \bar{F}_{Z_A}\left(\mathcal{Z}_{TA}(z)\right) \, f_{Z_T}(z) \, \mathrm{d}z, \tag{25}$$

where $a_T(z) = \bar{F}_{Z_A}(\mathcal{Z}_{TA}(z))$ expresses the conditional T-association probability.

B. A-Association Probability

Trivially, the association probabilities are complementary, therefore

$$\mathcal{A}_A = 1 - \mathcal{A}_T \, .$$

Alternatively, the A-association probability can be computed as

$$\mathcal{A}_A = \mathbb{P}\left(Z_T > \mathcal{Z}_{AT}(Z_A)\right) = \int_{\max(0,-r^-)}^{r^+} \bar{F}_{Z_T}\left(\mathcal{Z}_{AT}(z)\right) f_{Z_A}(z)\,\mathrm{d}z. \quad (26)$$

Appendix D
Proof of Theorem 4

Let us first define the sets of the C-BSs as $\check{\Phi}_C = \Phi_C \backslash (\mathcal{B}_z(\mathcal{Z}_{BM}(z)) \cup W^*)$, where $\mathcal{B}(z)$ denotes the circle of radius z centered around the typical user. Now, we can denote the set of TBSs' coordinates as $\mathbf{Y}$ and recall that $\mathcal{I}_T(s|\omega) = 1 - \left(\frac{m_T}{m_T + \xi_T\, s\, \mathcal{D}_{TT}^{-\alpha_T}(\omega)}\right)^{m_T}$. In order to obtain the expression of the conditional Laplace transform of the terrestrial interference, we firstly take the expectation over both the point process and the set of fading gains [28, Section III-C]:

$$\begin{aligned}\mathcal{L}_{I_{BT}}(s|z) &= \mathbb{E}\left[e^{-s\,I_{BT}}|z\right] \overset{(a)}{=} \mathbb{E}_{\Phi_T}\left[\prod_{Y_i \in \check{\Phi}_T} \psi_T(s, Y_i)\right] \\ &\overset{(b)}{=} \exp\left(-\int_{\mathbb{R}^2 \backslash \mathcal{B}_z(\mathcal{Z}_{BT}(z))} \lambda_T(\|\mathbf{Y}\|) \times \left(1 - \psi_T(s, \mathbf{Y})\right) \mathrm{d}\mathbf{Y}\right) \\ &= \exp\left(-\int_0^{2\pi} \int_{\mathcal{Z}_{BT}(z)}^{\infty} \lambda_T\left(r_\Omega(\check{\omega}, \beta)\right) \times \mathcal{I}_T(s|\check{\omega})\, \check{\omega}\, \mathrm{d}\check{\omega}\, \mathrm{d}\beta\right). \end{aligned} \quad (27)$$

Note that (a) follows from the independence of the exponentially distributed gains G_{T,Y_i}'s, having introduced the function $\psi_C(s, W_i) = \mathbb{E}_{G_{C,W_i}}\left[\exp\left(-\frac{s\, G_{C,W_i}\, \xi_C}{\|W_i\|^{\alpha_C}}\right)\right]$ for any type of interferers, and (b) derives from the application of the probability generating functional (PGFL) to the latter function.

Appendix E
Proof of Theorem 5

By letting $\check{\Omega}_A$ denote the set of aerial interferers' horizontal distances and recalling that $\check{N}_A = N_A - \mathbb{1}(B = A)$, the Laplace transform of the aerial interference conditioned on B-association can be derived as [28, (4), (16)]

$$\begin{aligned}\mathcal{L}_{I_{BA}}(s|z) &= \mathbb{E}_{I_{BA}}\left[e^{-s\,I_{BA}}|z\right] = \mathbb{E}_{I_{BA}}\left[\exp\left(-s\sum_{i=1}^{\check{N}_A} G_i\, \mathcal{D}_{AA}^{-\alpha_A}(\check{\Omega}_{A,i})\right)|z\right] \\ &\overset{(a)}{=} \mathbb{E}_{\check{\Omega}_A}\left[\mathbb{E}_G\left[\prod_{i=1}^{\check{N}_A} \exp\left(-s\, G_i\, \mathcal{D}_{AA}^{-\alpha_A}(\check{\Omega}_{A,i})\right)|z\right]\right] \\ &\overset{(b)}{=} \mathbb{E}_{\check{\Omega}_A}\left[\prod_{i=1}^{\check{N}_A} \mathbb{E}_{G_i}\left[\exp(-s\, G_i\, \mathcal{D}_{AA}^{-\alpha_A}(\check{\Omega}_{A,i}))\right]|z\right] \\ &\overset{(c)}{=} \mathbb{E}_{\check{\Omega}_A}\left[\prod_{i=1}^{\check{N}_A} \mathcal{I}_{A,i}(s|\check{\Omega}_{A,i})|z\right] \\ &\overset{(d)}{=} \left(\mathbb{E}_{\check{\Omega}_{A,i}}\left[\mathcal{I}_{A,i}(s|\check{\Omega}_{A,i})|z\right]\right)^{\check{N}_A}, \end{aligned} \quad (28)$$

where $\mathcal{I}_{A,i}(s|\check{\Omega}_{A,i}) = \left(\frac{m_A}{m_A + \xi_A\, s\, \mathcal{D}_{AA}^{-\alpha_A}(\check{\Omega}_{A,i})}\right)^{m_A}$. Step (a) follows from the independence of the channel gains and the distances of the aerial interferers, whereas (b) follows from rewriting the expectation of a product as a product of the expectations owing to iid channel gains. Then, (c) follows from the moment generating function (MGF) of the gamma-distributed fading gains G_i's [25, Appendix E], and (d) from the conditional iid distances of the aerial interferers.

Appendix F
Proof of Theorem 6

Let us first recall from Table II and Theorem 3 the expressions of the Euclidean distances $\mathcal{D}_{BB}(z)$'s and the planar domains $\mathcal{R}_B$'s, respectively. Now, following the same approach proposed in [29], the exact expression of the coverage probability can be obtained as

$$\begin{aligned}P_c &= \mathbb{E}_{Z_B}\left[\mathbb{P}(\mathrm{SINR} > \tau \,|\, Z_B = z)\right] \\ &= \sum_{B=\{A,T\}} \mathbb{E}_{Z_B}\left[a_B(Z_B)\, p_{c,B}(Z_B)\right] \\ &= \sum_{B=\{A,T\}} \int_{\mathcal{R}_B} a_B(z)\, p_{c,B}(z)\, f_{Z_B}(z)\,\mathrm{d}z, \end{aligned} \quad (29)$$

in which the exact expressions of the conditional coverage probabilities are given by[3]

$$\begin{aligned}p_{c,B}(z) &= \mathbb{P}\left(\frac{\xi_B\, G_B^*\, \mathcal{D}_{BB}^{-\alpha_B}(z)}{J} > \tau\right) \\ &= \mathbb{P}\left(G_B^* > \frac{\tau\, J}{\xi_B\, \mathcal{D}_{BB}^{-\alpha_B}(z)}\right), \end{aligned} \quad (30)$$

with $J = \sigma_n^2 + I$. By definition, the CCDF of the Gamma distribution is $\bar{F}_G(g) = \frac{\Gamma^u(m, m\,g)}{\Gamma(m)}$, where $\Gamma^u(m, m\,g) = \int_{m\,g}^{\infty} t^{m-1}\, e^{-t}\,\mathrm{d}t$ is the upper incomplete Gamma function. Let $\mu_B(z) = m_B\, \frac{\tau}{\xi_B}\, \mathcal{D}_{BB}^{\alpha_B}(z)$, taking the expectation with respect to J implies that [20]

$$p_{c,B}(z) = \mathbb{E}_J\left[\frac{\Gamma^u\left(m_B, \mu_B(z)\, J\right)}{\Gamma(m_B)}\right]$$

[3] In the particular case of Rayleigh fading channel ($m_B = 1$), we can compute the conditional coverage probability as $p_{c,B}(z) = \exp\left(-\frac{\tau\, \mathcal{D}_{BB}^{\alpha_B}(z)\, \sigma_n^2}{\xi_B}\right) \mathcal{L}_{I,B}\left(\frac{\tau\, \mathcal{D}_{BB}^{\alpha_B}(z)}{\xi_B}, z\right)$.

$$\overset{(a)}{=} \mathbb{E}_J\left[e^{-\mu_B(z)\,J}\sum_{k=0}^{m_B-1}\frac{(\mu_B(z)\,J)^k}{k!}\right]$$

$$\overset{(b)}{=} \sum_{k=0}^{m_B-1}\frac{\mu_B^k(z)}{k!}\,\mathbb{E}_J\left[e^{-\mu_B(z)\,J}\,J^k\right], \qquad (31)$$

where (a) follows from the definition $\frac{\Gamma^u(m,g)}{\Gamma(m)} = e^{-g}\sum_{k=0}^{m-1}\frac{g^k}{k!}$, and (b) is obtained from the linearity of the expectation operator. Taking into account that

$$\mathbb{E}_J\left[e^{-s\,J}\,J^k\right] = (-1)^k\,\frac{\partial^k}{\partial s^k}\,\mathcal{L}_J(s|z),$$

where

$$\mathcal{L}_J(s|z) = \mathbb{E}\left[e^{-s\,J}\right] = \mathbb{E}\left[e^{-s\,I}\,e^{-s\sigma_n^2}\right]$$

$$= e^{-s\,\sigma_n^2}\,\mathbb{E}\left[e^{-s\,I}\right] = e^{-s\,\sigma_n^2}\,\mathcal{L}_I(s|z),$$

the final expression is obtained. This, however, may require the computation of high-order derivatives of the conditional Laplace transform of the interference, resulting in a number of terms proportional to m_B.

Appendix G
Proof of Theorem 7

A tight bound can be applied to the CDF of the Gamma distribution in order to ease the computation of the conditional coverage probabilities provided in Theorem 6. Let $\Gamma_l(m, m\,g) = \int_0^{m\,g} t^{m-1}\,e^{-t}\,\mathrm{d}t$ denote the lower incomplete Gamma function, then the CDF of the Gamma distribution $F_G(g) = \frac{\Gamma_l(m,\,m\,g)}{\Gamma(m)} = 1 - \frac{\Gamma^u(m,\,m\,g)}{\Gamma(m)}$, can be bounded as [30]

$$(1-e^{-\varepsilon_1\,m\,g})^m \le \frac{\Gamma_l(m,m\,g)}{\Gamma(m)} \le (1-e^{-\varepsilon_2\,m\,g})^m,$$

where we defined the constants $\varepsilon_1 = \begin{cases}1, & \text{if } m \ge 1\\ (m!)^{-\frac{1}{m}}, & \text{if } m < 1\end{cases}$ and $\varepsilon_2 = \begin{cases}(m!)^{-\frac{1}{m}}, & \text{if } m > 1\\ 1, & \text{if } m \le 1\end{cases}$.

Note that for $m = 1$ the upper and the lower bounds become equal and thus $\frac{\Gamma_l(1,g)}{\Gamma(1)} = 1 - e^{-g}$. It has been shown in [31] that the upper bound actually is a good approximation, hence we consider $\varepsilon_2 = (m!)^{-\frac{1}{m}}$.

Recalling that $\mu_B(z) = m_B\,\frac{\tau}{\xi_B}\,\mathcal{D}_{BB}^{\alpha_B}(z)$, the conditional coverage probabilities can be approximated as [20, Appendix F]

$$p_{c,B} = \mathbb{E}_J\left[\frac{\Gamma^u(m_B,\mu_B(z)\,J)^k}{\Gamma(m_B)}\right]$$

$$= \mathbb{E}_J\left[1-\frac{\Gamma_l(m_B,\mu_B(z)\,J)}{\Gamma(m_B)}\right]$$

$$\overset{(a)}{\approx} 1-\mathbb{E}_J\left[\left(1-e^{-\varepsilon_{2,B}\,\mu_B(z)\,J}\right)^{m_B}\right]$$

$$\overset{(b)}{=} 1-\mathbb{E}_J\left[\sum_{k=0}^{m_B}\binom{m_B}{k}(-1)^{m_B-k}\left(-e^{-\varepsilon_{2,B}\,\mu_B(z)\,J}\right)^k\right]$$

$$= \mathbb{E}_J\left[\sum_{k=1}^{m_B}\binom{m_B}{k}(-1)^{k+1}\,\exp(-k\,\varepsilon_{2,B}\,\mu_B(z)\,J)\right]$$

$$= \sum_{k=1}^{m_B}\binom{m_B}{k}(-1)^{k+1}\,\mathbb{E}_J\left[\exp\left(-k\,\varepsilon_{2,B}\,\mu_B(z)\,J\right)\right], \qquad (32)$$

where (a) follows from the upper bound previously introduced and (b) from the binomial theorem under the assumption that $m_B \in \mathbb{N}$. The final result in (21) can be obtained by applying the definition of the conditional Laplace transform of the interference.

References

[1] United Nations Office for Coordination of Humanitarian Affairs (UNOCHA), "The Story of INSARAG 20 Years On...," 2010.

[2] C. Esposito, Z. Zhao, and J. Rak, "Reinforced secure gossiping against DoS attacks in post-disaster scenarios," *IEEE Access*, vol. 8, pp. 178651–178669, 2020.

[3] M. Matracia, N. Saeed, M. A. Kishk, and M.-S. Alouini, "Post-disaster communications: Enabling technologies, architectures, and open challenges," *IEEE Open J. Commun. Soc.*, vol. 3, pp. 1177–1205, 2022.

[4] M. Matracia, M. A. Kishk, and M.-S. Alouini, "On the topological aspects of UAV-assisted post-disaster wireless communication networks," *IEEE Commun. Mag.*, vol. 59, no. 11, pp. 59–64, Nov. 2021.

[5] M. Mozaffari, W. Saad, M. Bennis, Y. Nam, and M. Debbah, "A tutorial on UAVs for wireless networks: Applications, challenges, and open problems," *IEEE Commun. Surveys Tuts.*, vol. 21, no. 3, pp. 2334–2360, Jul.–Sep. 2019.

[6] A. Al-Hourani, S. Kandeepan, and S. Lardner, "Optimal LAP altitude for maximum coverage," *IEEE Wireless Commun. Lett.*, vol. 3, no. 6, pp. 569–572, Dec. 2014.

[7] A. V. Savkin and H. Huang, "Navigation of a network of aerial drones for monitoring a frontier of a moving environmental disaster area," *IEEE Syst. J.*, vol. 14, no. 4, pp. 4746–4749, Dec. 2020.

[8] W. Wu, M. A. Qurishee, J. Owino, I. Fomunung, M. Onyango, and B. Atolagbe, "Coupling deep learning and UAV for infrastructure condition assessment automation," in *Proc. IEEE Int. Smart Cities Conf.*, Kansas City, Missouri, USA, 2018, pp. 1–7.

[9] P. Sanjana and M. Prathilothamai, "Drone design for first aid kit delivery in emergency situation," in *Proc. 6th Int. Conf. Adv. Comput. Commun. Syst.*, Piscataway, NJ, USA, 2020, pp. 215–220.

[10] M. Kishk, A. Bader, and M.-S. Alouini, "Aerial base station deployment in 6G cellular networks using tethered drones: The mobility and endurance tradeoff," *IEEE Veh. Technol. Mag.*, vol. 15, no. 4, pp. 103–111, Dec. 2020.

[11] M. A. Kishk, A. Bader, and M.-S. Alouini, "On the 3-D placement of airborne base stations using tethered UAVs," *IEEE Trans. Commun.*, vol. 68, no. 8, pp. 5202–5215, Aug. 2020.

[12] M. Erdelj and E. Natalizio, "UAV-assisted disaster management: Applications and open issues," in *Proc. IEEE Int. Conf. Comput. Netw. Commun.*, Kauai, Hawaii, USA, 2016, pp. 1–5.

[13] O. H. Graven, J.-V. Sørli, J. Bjørk, D. A. H. Samuelsen, and J. D. Bjerknes, "Managing disasters-rapid deployment of sensor network from drones: Providing first responders with vital information," in *Proc. IEEE 2nd Int. Conf. Control Robot. Eng.*, Bangkok, Thailand, 2017, pp. 184–188.

[14] C. A. F. Ezequiel et al., "UAV aerial imaging applications for post-disaster assessment, environmental management and infrastructure development," in *Proc. IEEE Int. Conf. Unmanned Aircr. Syst.*, Orlando, Florida, USA, 2014, pp. 274–283.

[15] S. A. R. Naqvi, S. A. Hassan, H. Pervaiz, and Q. Ni, "Drone-aided communication as a key enabler for 5G and resilient public safety networks," *IEEE Commun. Mag.*, vol. 56, no. 1, pp. 36–42, Jan. 2018.

[16] M. Y. Selim and A. E. Kamal, "Post-disaster 4 G/5G network rehabilitation using drones: Solving battery and backhaul issues," in *Proc. IEEE Globecom Workshops*, Abu Dhabi, UAE, 2018, pp. 1–6.

[17] S. Shakoor, Z. Kaleem, M. I. Baig, O. Chughtai, T. Q. Duong, and L. D. Nguyen, "Role of UAVs in public safety communications: Energy efficiency perspective," *IEEE Access*, vol. 7, pp. 140665–140679, 2019.

[18] R. Masroor, M. Naeem, and W. Ejaz, "Efficient deployment of UAVs for disaster management: A multi-criterion optimization approach," *Comput. Commun.*, vol. 177, pp. 185–194, 2021.
[19] R. Arshad, L. Lampe, H. ElSawy, and M. J. Hossain, "Integrating UAVs into existing wireless networks: A stochastic geometry approach," in *Proc. IEEE Globecom Workshops*, Abu Dhabi, UAE, 2018, pp. 1–6.
[20] M. Alzenad and H. Yanikomeroglu, "Coverage and rate analysis for vertical heterogeneous networks (VHetNets)," *IEEE Trans. Wireless Commun.*, vol. 18, no. 12, pp. 5643–5657, Dec. 2019.
[21] M. Matracia, M. A. Kishk, and M.-S. Alouini, "Coverage analysis for UAV-assisted cellular networks in rural areas," *IEEE Open J. Veh. Technol.*, vol. 2, pp. 194–206, 2021.
[22] N. Kouzayha, H. ElSawy, H. Dahrouj, K. Alshaikh, T. Y. Al-Naffouri, and M.-S. Alouini, "Stochastic geometry analysis of hybrid aerial terrestrial networks with mmWave backhauling," in *Proc. IEEE Int. Conf. Commun.*, Dublin, Ireland, 2020, pp. 1–7.
[23] A. M. Hayajneh, S. A. R. Zaidi, D. C. McLernon, M. Di Renzo, and M. Ghogho, "Performance analysis of UAV enabled disaster recovery networks: A stochastic geometric framework based on cluster processes," *IEEE Access*, vol. 6, pp. 26215–26230, 2018.
[24] M. Afshang and H. S. Dhillon, "Fundamentals of modeling finite wireless networks using binomial point process," *IEEE Trans. Wireless Commun.*, vol. 16, no. 5, pp. 3355–3370, May 2017.
[25] V. V. Chetlur and H. S. Dhillon, "Downlink coverage analysis for a finite 3-D wireless network of unmanned aerial vehicles," *IEEE Trans. Commun.*, vol. 65, no. 10, pp. 4543–4558, Oct. 2017.
[26] J. G. Andrews, F. Baccelli, and R. K. Ganti, "A tractable approach to coverage and rate in cellular networks," *IEEE Trans. Commun.*, vol. 59, no. 11, pp. 3122–3134, Nov. 2011.
[27] M. Haenggi, *Stochastic Geometry for Wireless Networks*. New York, NY, USA: Cambridge Univ. Press, 2012.
[28] J. G. Andrews, A. K. Gupta, and H. S. Dhillon, "A primer on cellular network analysis using stochastic geometry," 2016. [Online]. Available: https://arxiv.org/abs/1604.03183
[29] B. Galkin, J. Kibilda, and L. A. DaSilva, "A stochastic model for UAV networks positioned above demand hotspots in urban environments," *IEEE Trans. Veh. Technol.*, vol. 68, no. 7, pp. 6985–6996, Jul. 2019.
[30] H. Alzer, "On some inequalities for the incomplete gamma function," *Math. Comput.*, vol. 66, no. 218, pp. 771–778, 1997.
[31] T. Bai and R. W. Heath, "Coverage and rate analysis for millimeter-wave cellular networks," *IEEE Trans. Wireless Commun.*, vol. 14, no. 2, pp. 1100–1114, Feb. 2015.

Maurilio Matracia (Student Member, IEEE) received the M.Sc. degree in electrical engineering from the University of Palermo, Palermo, Italy, in 2019. He is currently working toward the Doctoral degree with the Communication Theory Lab, King Abdullah University of Science and Technology (KAUST), Kingdom of Saudi Arabia (KSA), Thuwal, Saudi Arabia. His main research interest include stochastic geometry, with a special focus on rural and emergency communications.

Mustafa A. Kishk (Member, IEEE) received the B.Sc. and M.Sc. degrees in electrical engineering from Cairo University, Giza, Egypt, in 2013 and 2015, respectively, and the Ph.D. degree in electrical engineering from Virginia Tech, Blacksburg, VA, USA, in 2018. He is currently an Assistant Professor with Electronic Engineering Department, Maynooth University, Maynooth, Ireland. He was a Postdoctoral Research Fellow with the Communication Theory Laboratory, King Abdullah University of Science and Technology, Thuwal, Saudi Arabia. He is also an Associate Editor for IEEE WIRELESS COMMUNICATION LETTERS. His research interests include stochastic geometry, UAV-enabled communication systems, and satellite-enabled communications. He was the recipient of the IEEE ComSoc Outstanding Young Researcher Award for Europe, Middle East, and Africa Region, in 2022, and was recognized as an Exemplary Reviewer by the IEEE COMMUNICATIONS LETTERS in 2020 and 2021.

Mohamed-Slim Alouini (Fellow, IEEE) was born in Tunis, Tunisia. He received the Ph.D. degree in electrical engineering from the California Institute of Technology, Pasadena, CA, USA. He was a Faculty Member with the University of Minnesota, Minneapolis, MN, USA, and Texas A&M University at Qatar, Education City, Doha, Qatar, before joining King Abdullah University of Science and Technology, Thuwal, Saudi Arabia, as a Professor of electrical engineering in 2009. His research interests include modeling, design, and performance analysis of wireless communication systems.